Editors' Suggestion | Featured in Physics

Current-Induced Creation of Topological Vortex Rings in a Magnetic Nanocylinder

Yizhou Liu and Naoto Nagaosa
RIKEN Center for Emergent Matter Science (CEMS), Wako, Saitama 351-0198, Japan

(Received 29 October 2023; revised 22 January 2024; accepted 29 January 2024; published 19 March 2024)

Vortex rings are ubiquitous topological structures in nature. In solid magnetic systems, their formation leads to intriguing physical phenomena and potential device applications. However, realizing these topological magnetic vortex rings and manipulating their topology on demand have still been challenging. Here, we theoretically show that topological vortex rings can be created by a current pulse in a chiral magnetic nanocylinder with a trench structure. The creation process involves the formation of a vortex ring street, i.e., a chain of magnetic vortex rings with an alternative linking manner. The created vortex rings can be bounded with monopole-antimonopole pairs and possess a rich and controllable linking topology (e.g., Hopf link and Solomon link), which is determined by the duration and amplitude of the current pulse. Our proposal paves the way for the realization and manipulation of diverse three-dimensional (3D) topological spin textures and could catalyze the development of 3D spintronic devices.

DOI: 10.1103/PhysRevLett.132.126701

Topological spin textures with real space topology such as skyrmions in two-dimensional (2D) systems have gained much attention due to both their fascinating physical properties and potential in information applications [1–3]. Extending to three-dimensional (3D) systems, the addition of a third spatial dimension further enriches topological spin textures with diverse topology such as rings, links, and knots [4–7]. Because of their 3D nature, these 3D topological spin textures like magnetic hopfions host sophisticated spin structures and the corresponding 3D emergent magnetic fields lead to interesting dynamical properties (e.g., current-driven dynamics and nonlinear transport responses [8–11]) and novel device applications [12–14].

Vortex rings are common 3D structures in a variety of natural systems, from cosmology to biology [15–21]. Although mostly discussed in fluid dynamics, other physical systems (e.g., liquid crystal and Bose-Einstein condensate) can also form vortex ring structure with an effective vorticity defined therein [22–25]. Magnetic vortex rings are formed by localized spins in 3D magnetic systems. They are characterized by the magnetic vorticity $B_i^e(\mathbf{r}) = \frac{1}{2}\epsilon_{ijk}\mathbf{S}\cdot(\partial_j\mathbf{S}\times\partial_k\mathbf{S})$ ($\mathbf{S}$ is the unit vector of spin), which is also the emergent magnetic field and whose 2D integral is the topological skyrmion number [1,26]. Magnetic vortex rings have been theoretically predicted as a dynamical state propagating in an analogous to a smoke ring [27–29]. Furthermore, they also exhibit a nontrivial link and knot topology as described by the Hopf charge, i.e., they are a class of magnetic hopfions [30–33]. Recently, stable magnetic vortex rings with trivial topology have been experimentally observed in bulk ferromagnets [34]. However, the creation and manipulation of topological magnetic vortex rings on demand have not been well explored so far, making further investigations into their emergent properties challenging.

Here, we theoretically show that magnetic vortex rings with diverse linking structures can be created using a current pulse in a chiral magnetic nanocylinder with a trench structure. The creation process involves a dynamical 3D vortex ring street [35], i.e., a chain of magnetic vortex rings with an alternative linking manner. Owing to the rich energy landscape of 3D chiral magnets [30,36–39], the created vortex rings possess various linking topology such as the Hopf link and the Solomon link, and they are also bounded with emergent magnetic monopole and antimonopole pairs. The topology of the created vortex rings are controlled by the duration and amplitude of the current pulse, thus providing a method to create 3D topological linking structures on-demand.

Creating a magnetic vortex ring with linking structure is associated with a change in the system's Hopf charge $Q_H = \int \mathbf{A}^e(\mathbf{r})\cdot\mathbf{B}^e(\mathbf{r})dV$ ($\mathbf{A}^e$ is the corresponding vector potential, $\mathbf{B}^e = \nabla\times\mathbf{A}^e$). In the absence of singularity, the change of Q_H as a function of time t can be derived as $dQ_H/dt = -\oint dS\Phi^e(\mathbf{B}^e\cdot\mathbf{n})$, where $\mathbf{n}$ is the unit vector pointing out of the sample surface and Φ^e is the emergent scalar potential associated with the emergent electric field $E_i^e(\mathbf{r}) = \frac{1}{2}\mathbf{S}\cdot(\partial_i\mathbf{S}\times\partial_t\mathbf{S}) = -\nabla\Phi^e - \partial\mathbf{A}^e/\partial t$ (for details of the derivation, see Supplemental Material [40]). This suggests that inducing spin dynamics at the boundary of the system can be employed for creating topological spin textures with finite Q_H. In this sense, a current pulse may serve as a proper driving force since it induces spin dynamics via the spin transfer torque (STT) [48–50]. On the other hand, the stability of a magnetic vortex ring is enhanced in a confined geometry [30]. Therefore, we

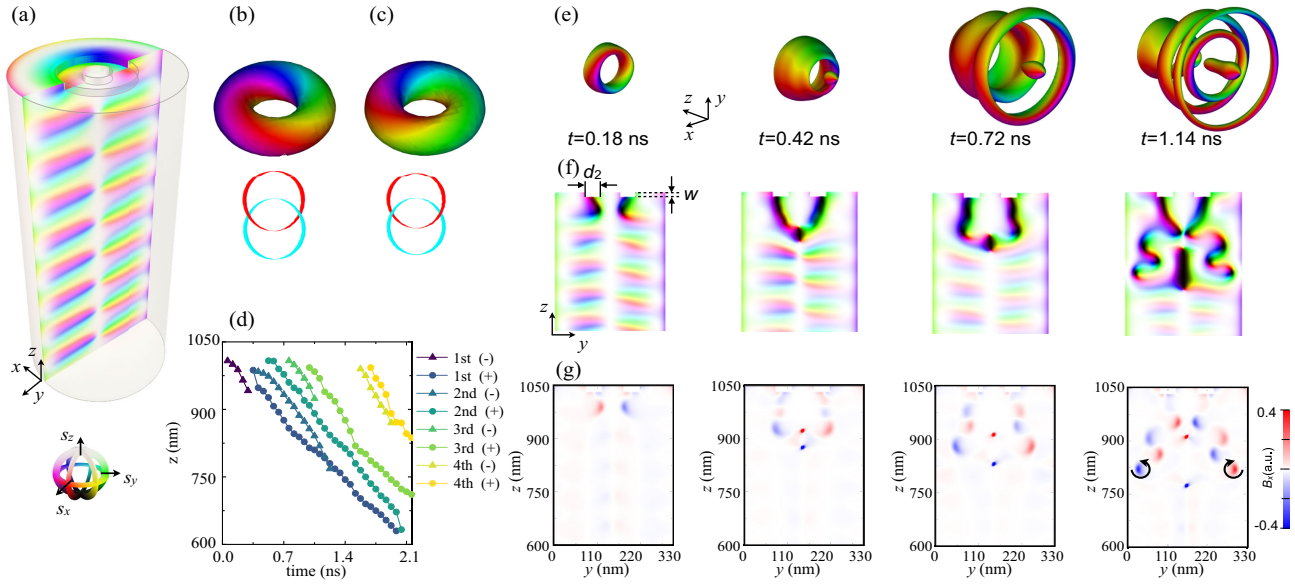

FIG. 1. Dynamical vortex ring creation. (a) Schematic view of the chiral magnetic nanocylinder with a trench structure on its top surface. The cross-sectional cut shows the conical state with screw dislocation. The bottom color wheel illustrates the color scheme that encodes the spin direction in three dimensions. (b),(c) Magnetic vortex ring with positive (b) and negative (c) linking. Top row is the equispin surface for $S_z = 0$. Bottom row is the linking of equispin lines with $S_x = 1$ (red) and $S_x = -1$ (cyan). (d) The created vortex rings' positions as a function of time. Termination of the line indicates the transformation and annihilation of the vortex ring. (e) Bird's eye view of the screenshots for the creation process at $0.5B_c$. Equispin surface with $S_z = -0.4$ is plotted. The applied current density is 5×10^{11} A/m^2. (f) Cross-sectional cut of the spin texture at the y-z plane corresponding to the screenshots in (e). (g) Cross-sectional cut of the emergent magnetic field's out-of-plane component associated with the created spin texture at different times. The amplitudes of the emergent magnetic field (B_x) for the monopole and antimonopole are artificially reduced by a factor of 0.1 to better visualize B_x for the other part of the spin texture. The black arrows in (g) indicate the rotating manner of the spin texture.

consider a chiral magnetic cylinder with a trench structure on its top surface as shown in Fig. 1(a) and employ a current pulse to create the magnetic vortex rings.

In the continuum approximation, the Hamiltonian density of a chiral magnet can be written as

$$\mathcal{H} = A(\nabla \mathbf{S})^2 - D\mathbf{S} \cdot (\nabla \times \mathbf{S}) - \mu_0 M_s \mathbf{B} \cdot \mathbf{S} \qquad (1)$$

where A is the strength of the Heisenberg exchange interaction, D is the strength of the Dzyaloshinskii-Moriya interaction, M_s is the saturation magnetization, and the last term is the Zeeman effect due to the external magnetic field $\mathbf{B}$. The corresponding helical period λ is determined by $4\pi A/D$, which is about 70 nm in the current study. The critical field to induce the field polarized state $B_c = D^2/2M_sA$ is about 0.4 T. For a fixed external magnetic field, the vortex rings can have two opposite linking manners [Figs. 1(b) and 1(c)], which are linked via the inversion operator (i.e., they also have opposite Hopf charge). In a centrosymmetric system (e.g., frustrated magnet with only competing exchange interactions [6,33]), magnetic vortex rings with both linking manners are degenerate states. In contrast, the chiral magnet favors a given chirality, so the magnetic vortex ring with preferable linking manner [positive linking manner for the current study, Fig. 1(c)] is more stable.

The initial magnetic state for the vortex ring creation is a conical state with screw dislocation stabilized by a $0.5B_c$ external magnetic field [51] as shown in Fig. 1(a). The radius (R) and length (L) of the cylinder are about 2.3λ and 14λ, respectively. For the trench structure, its width [d_2, defined in Fig. 1(f)] and depth (w) are 0.64λ and 0.43λ, respectively. These geometrical parameters are crucial for the creation of vortex rings, which will be discussed later.

To create magnetic vortex rings, a current pulse is injected into the nanocylinder and drives the spin dynamics via the STT effect (for simulation details, see Supplemental Material [40]). Once the current is applied, magnetic vortex rings are created sequentially as shown in Figs. 1(d)–1(g) (for an example of the complete dynamical process, see Supplemental Material movie [40]). Initially, a magnetic vortex ring with negative linking manner is created [Fig. 1(e) at $t = 0.18$ ns]. Its current-driven dynamics is similar to that of a hopfion, i.e., moving along the current direction with a dilation (shrinking here based on its linking manner) [9]. Moreover, as the chiral magnet favors the positive linking manner, this vortex ring is not stable and transformed into a monopole-antimonopole pair (MAP) at a later time [Figs. 1(e)–1(g) at $t = 0.42$ ns] [30,52]. In contrast, the second vortex ring is created with positive linking manner, which is favored by the chirality of the system and is more stable. However, since the expansion

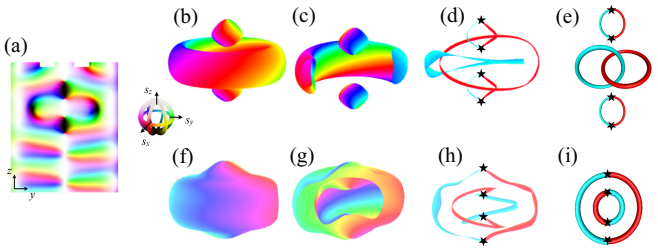

FIG. 2. Created spin texture with one vortex ring and two monopole-antimonopole pairs (MAPs). (a) Cross-sectional cut of the spin texture at the y-z plane. (b) Equispin surface for $S_z = 0$ of the created spin texture. (c) Cross-sectional cut of (b) showing the vortex ring and MAP structure. (d) Equispin lines with $\mathbf{S} = (1, 0, 0)$ (red) and $\mathbf{S} = (-1, 0, 0)$ (cyan) associated with (b). (e) Schematic linking structures for the equispin lines in (d). (f)–(i) Corresponding plots for equispin surface with $S_z = 0.4$ and equispin lines with $\mathbf{S} \approx (0.92, 0, 0.4)$ (light red) and $\mathbf{S} \approx (-0.92, 0, 0.4)$ (light cyan). Up (down) star symbol represents the monopole (antimonopole).

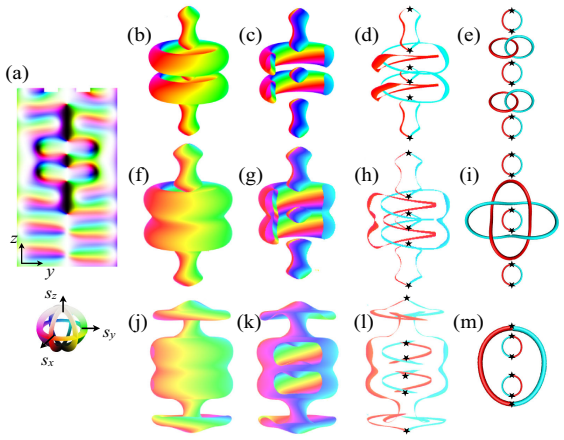

FIG. 3. Created spin texture with two vortex rings and three MAPs. (a) Cross-sectional cut of the spin texture at the y-z plane. (b) Equispin surface ($S_z = 0$) of the created spin texture. (c) Cross-sectional cut of (b) showing the vortex ring and MAP structure. (d) Equispin lines with $\mathbf{S} = (1, 0, 0)$ (red) and $\mathbf{S} = (-1, 0, 0)$ (cyan) associated with (b). (e) Schematic linking structures for the equispin lines in (d). (f)–(i) The corresponding plots for equispin surface with $S_z = 0.2$ and equispin lines with $\mathbf{S} \approx (0.98, 0, 0.2)$ (red) and $\mathbf{S} \approx (-0.98, 0, 0.2)$ (cyan). (j)–(m) The corresponding plots for equispin surface with $S_z = 0.4$ and equispin lines with $\mathbf{S} \approx (0.92, 0, 0.4)$ (red) and $\mathbf{S} \approx (-0.92, 0, 0.4)$ (cyan). (e),(i),(m) Up (down) star symbol represents the monopole (antimonopole).

mode is associated with its translational motion, as the vortex ring keeps moving, it is going to hit the boundary of the cylinder and gets annihilated [Fig. 1(d) and Supplemental Material Fig. S1 [40]).

At a later time, the magnetic vortex rings with opposite linking manners are created alternatively, which resembles a dynamical 3D vortex ring street [35]. This process is also clearly indicated by the emergent magnetic field of the spin texture [Fig. 1(g)], where the vortex rings with opposite chirality can be readily distinguished by the opposite emergent magnetic field at their cross sections. Furthermore, as the created magnetic vortex rings with negative linking manner keep transforming into MAPs, the merging of MAPs also happens as the monopole and animonopole attract each other (Supplemental Material Fig. S2 [40]).

After turning off the current, the created vortex rings do not vanish but rather relax into diverse topological states depending on the applied current pulse amplitude and duration. Figure 2 shows a typical spin texture created by a 0.75 ns current pulse with an amplitude 5×10^{11} A/m^2. As the current duration is short, the spin texture is formed near the top surface. For $S_z < 0.3$, the created spin texture shows a vortex ring sandwiched by two MAPs as illustrated by the equispin surface [plotted for $S_z = 0$, Figs. 2(b) and 2(c)]. Figures 2(d) and 2(e) show the corresponding equispin lines plot and the schematic linking diagram. For the vortex ring, its equispin lines are closed and linked once, while for the MAPs their equispin lines are connected at the monopole and antimonopole. As we further scan the equispin surface, for $S_z > 0.3$, the topology changes to two concentric MAPs [Figs. 2(f) and 2(g)]. The corresponding equispin lines unlink the vortex ring and reconnect the top most monopole (antimonopole) to the bottom most antimonopole (monopole) as shown in Figs. 2(h) and 2(i), giving rise to the concentric MAP structure. Therefore, the created vortex ring is also bounded with the MAPs.

Figure 3 shows another topological vortex ring structure created by a 1 ns current pulse with an amplitude 5×10^{11} A/m^2. For $S_z < 0.1$, the equispin surface consists of two magnetic vortex rings and three MAPs [Figs. 3(b)–3(e)]. Each magnetic vortex ring is sandwiched by two MAPs. It is noted that the MAPs have different lengths which are quantized in λ. These MAPs with different lengths are metastable states protected by a finite energy barrier [39] and their lengths are closely related to the current pulse duration. As shown by the schematic linking diagram [Figs. 3(d) and 3(e)], the MAPs and the linking of vortex rings can be clearly seen for $S_z < 0.1$. The topology of the equispin surface changes at $S_z \approx 0.1$ [Figs. 3(f)–3(i)]. The two magnetic vortex rings merged into a single vortex ring with higher order linking [Figs. 3(f) and 3(g)] while the three MAPs still keep their topology. The linking diagrams [Figs. 3(h) and 3(i)] suggest that the equispin surfaces possess Solomon link where its equispin lines linked twice. For $S_z > 0.4$, the spin texture transforms into two MAPs wrapped by a large deformed MAP as shown by Figs. 3(j)–3(m). Similar to the case shown in Fig. 2, the equispin lines unlink the vortex ring and reconnect the monopoles and antimonopoles.

Topological vortex rings with even higher order linking can also be created by longer current pulses. Figure 4 summarizes the spin textures created by a 2 ns (a)–(d) and a 2.5 ns (e)–(h) current pulse with an amplitude

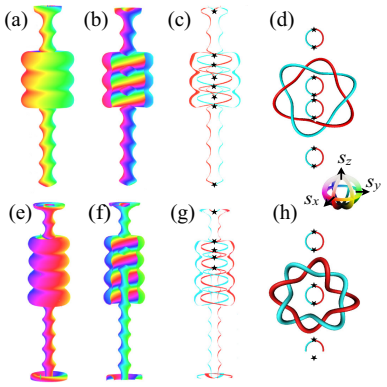

FIG. 4. Created spin texture with three (a)–(d) and four (e)–(h) vortex rings. (a),(e) Equispin surfaces ($S_z = 0.2$) of the created spin texture. (b),(f) Cross-sectional cuts of (a) and (e) showing the vortex ring and MAP structure. (c),(g) Equispin lines with $\mathbf{S} \approx (0.98, 0, 0.2)$ (red) and $\mathbf{S} \approx (-0.98, 0, 0.2)$ (cyan) associated with (a),(e). (d),(h) Schematic linking structures for the equispin lines shown in (c),(g). For clarity, the view point is modified based on different spin textures.

5×10^{11} A/m^2. For clarity, only the equispin surfaces for $S_z = 0.2$ with higher order linkings are shown (for complete analysis of these spin textures, see Supplemental Material Figs. S3 and S4). Upon applying a long enough current like 2.5 ns, the MAP also moves to the bottom surface and transforms into a chiral bobber [a skyrmion string terminated with a monopole, Fig. 4(f)]. For the three (four) vortex rings case, its equispin lines linked three (four) times. These created spin textures are also robust in the presence of reasonable disorders, edge roughness, and thermal fluctuations (Supplemental Material Sec. V).

The length and radius of the cylinder are crucial for the stable vortex ring creation. To create multiple vortex rings, the length and radius of the cylinder needs to be large enough as shown in Figs. 5(a) and 5(b). It is found a radius R around 3λ is optimized for generating the topological magnetic vortex rings [Figs. 5(c) and 5(d)]. If the radius of the cylinder is too large, the created vortex rings may become unstable due to the excitation of internal modes, e.g., Kelvin waves (see Supplemental Material Fig. S9 [40]). The magnetic field and the geometry of the trench also play roles in determining the creation of vortex ring (for details and a full phase diagram, see Supplemental Material Sec. VI).

For real experiments, the created topological spin textures can be checked by magnetic imaging techniques such as Lorentz transmission microscopy (LTEM) and x-ray microscopy [34,53,54]. Based on the created spin textures, the corresponding LTEM images are simulated for experimental references (see Supplemental Material Fig. S7 [40]), where the number of vortex rings can be identified. In addition, since the topological vortex rings could induce nonreciprocal magnetoresistance and nonlinear Hall effect [10], it is also possible to monitor their creation by transport measurements.

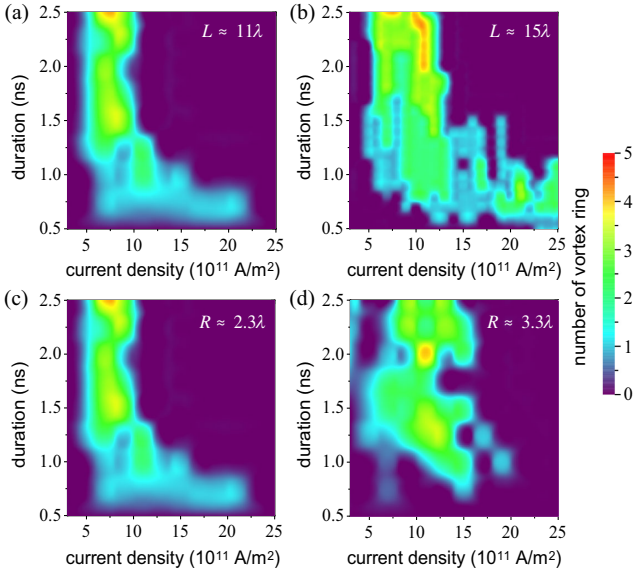

FIG. 5. Phase diagram of topological vortex ring creation as a function of current pulse amplitude and duration under various conditions. (a),(b) Phase diagrams for the cylinder with varying length at $B_z = 0.5B_c$ (other geometrical parameters are the same as that used in Fig. 1. (c),(d) Phase diagrams for the cylinder with varying radius at $B_z = 0.5B_c$ (with fixed length 11λ). The color bar indicates the number of vortex rings created.

In summary, we have proposed a method to create topological vortex rings on demand in a chiral magnetic nanocylinder. By injecting a current pulse through a "magnetic nozzle," topological vortex rings with diverse linking structures and their bound states with MAPs are created. The topology of the created spin texture is determined by the amplitude and duration of the current pulse. Our results provide a feasible method to experimentally create topological magnetic vortex rings. With proper driving force, this method might be applicable to other physical systems such as liquid crystals and Bose-Einstein condensates, where the multiple vortex ring states can also be stabilized. The created vortex ring state with MAPs would enable further investigations of their dynamical modes and transport phenomena, which could be rich due to their sophisticated 3D structures. Our proposal also provides a new way to manipulate 3D topological spin textures and could be useful for the development of unconventional 3D spintronic devices [12,14,55].

We thank W. Koshibae, M. Birch, and X. Yu for fruitful discussions. N. N. was supported by JST CREST Grant No. JMPJCR1874. Y. L. acknowledges support from the RIKEN Special Postdoctoral Researcher (SPDR) Program and JST CREST Grant No. JPMJCR20T1.

[1] N. Nagaosa and Y. Tokura, Nat. Nanotechnol. **8**, 899 (2013).
[2] A. Fert, N. Reyren, and V. Cros, Nat. Rev. Mater. **2**, 1 (2017).

[3] C. Reichhardt, C. J. O. Reichhardt, and M. V. Milošević, Rev. Mod. Phys. **94**, 035005 (2022).
[4] L. Faddeev and A. J. Niemi, Nature (London) **387**, 58 (1997).
[5] R. A. Battye and P. M. Sutcliffe, Phys. Rev. Lett. **81**, 4798 (1998).
[6] P. Sutcliffe, Phys. Rev. Lett. **118**, 247203 (2017).
[7] B. Göbel, I. Mertig, and O. A. Tretiakov, Phys. Rep. **895**, 1 (2021).
[8] X. S. Wang, A. Qaiumzadeh, and A. Brataas, Phys. Rev. Lett. **123**, 147203 (2019).
[9] Y. Liu, W. Hou, X. Han, and J. Zang, Phys. Rev. Lett. **124**, 127204 (2020).
[10] Y. Liu, H. Watanabe, and N. Nagaosa, Phys. Rev. Lett. **129**, 267201 (2022).
[11] C. Saji, R. E. Troncoso, V. L. Carvalho-Santos, D. Altbir, and A. S. Nunez, Phys. Rev. Lett. **131**, 166702 (2023).
[12] A. Fernández-Pacheco, R. Streubel, O. Fruchart, R. Hertel, P. Fischer, and R. P. Cowburn, Nat. Commun. **8**, 15756 (2017).
[13] C. Back, V. Cros, H. Ebert, K. Everschor-Sitte, A. Fert, M. Garst, T. Ma, S. Mankovsky, T. L. Monchesky, M. Mostovoy, N. Nagaosa, S. S. P. Parkin, C. Pfleiderer, N. Reyren, A. Rosch, Y. Taguchi, Y. Tokura, K. v. Bergmann, and J. Zang, J. Phys. D **53**, 363001 (2020).
[14] Z. Zhang, K. Lin, Y. Zhang, A. Bournel, K. Xia, M. Kläui, and W. Zhao, Sci. Adv. **9**, eade7439 (2023).
[15] E. Babaev, L. D. Faddeev, and A. J. Niemi, Phys. Rev. B **65**, 100512(R) (2002).
[16] G. Pedrizzetti and F. Domenichini, Phys. Rev. Lett. **95**, 108101 (2005).
[17] E. Radu and M. S. Volkov, Phys. Rep. **468**, 101 (2008).
[18] D. G. Akhmetov, *Vortex Rings* (Springer, Berlin, Heidelberg, 2009).
[19] D. Kleckner and W. T. M. Irvine, Nat. Phys. **9**, 253 (2013).
[20] Y. Li, X. Zhou, and C. Wu, Phys. Rev. A **93**, 033628 (2016).
[21] F. Cardano and L. Marrucci, Nat. Photonics **16**, 476 (2022).
[22] M. D. Reichl and E. J. Mueller, Phys. Rev. A **88**, 053626 (2013).
[23] D. S. Hall, M. W. Ray, K. Tiurev, E. Ruokokoski, A. H. Gheorghe, and M. Möttönen, Nat. Phys. **12**, 478 (2016).
[24] L.-K. Lim and R. Moessner, Phys. Rev. Lett. **118**, 016401 (2017).
[25] P. J. Ackerman and I. I. Smalyukh, Nat. Mater. **16**, 426 (2017).
[26] G. E. Volovik, J. Phys. C **20**, L83 (1987).
[27] N. Papanicolaou, in *Singularities in Fluids, Plasmas and Optics* (Springer Netherlands, Dordrecht, 1993), pp. 151–158.
[28] N. R. Cooper, Phys. Rev. Lett. **82**, 1554 (1999).
[29] P. Sutcliffe, Phys. Rev. B **76**, 184439 (2007).
[30] Y. Liu, R. K. Lake, and J. Zang, Phys. Rev. B **98**, 174437 (2018).
[31] J.-S. B. Tai and I. I. Smalyukh, Phys. Rev. Lett. **121**, 187201 (2018).
[32] P. Sutcliffe, J. Phys. A **51**, 375401 (2018).
[33] F. N. Rybakov, N. S. Kiselev, A. B. Borisov, L. Döring, C. Melcher, and S. Blügel, APL Mater. **10**, 111113 (2022).
[34] C. Donnelly, M. Guizar-Sicairos, V. Scagnoli, S. Gliga, M. Holler, J. Raabe, and L. J. Heyderman, Nature (London) **547**, 328 (2017).
[35] Y. Shen, N. Papasimakis, and N. I. Zheludev, arXiv:2204.05676.
[36] F. Zheng, F. N. Rybakov, A. B. Borisov, D. Song, S. Wang, Z.-A. Li, H. Du, N. S. Kiselev, J. Caron, A. Kovács, M. Tian, Y. Zhang, S. Blügel, and R. E. Dunin-Borkowski, Nat. Nanotechnol. **13**, 451 (2018).
[37] X. Yu, Y. Liu, K. V. Iakoubovskii, K. Nakajima, N. Kanazawa, N. Nagaosa, and Y. Tokura, Adv. Mater. **35**, 2210646 (2023).
[38] R. Voinescu, J.-S. B. Tai, and I. I. Smalyukh, Phys. Rev. Lett. **125**, 057201 (2020).
[39] G. P. Müller, F. N. Rybakov, H. Jónsson, S. Blügel, and N. S. Kiselev, Phys. Rev. B **101**, 184405 (2020).
[40] See Supplemental Material at http://link.aps.org/supplemental/10.1103/PhysRevLett.132.126701, which also includes Refs. [41–47], for the movie of the vortex ring creation, details of the derivations and numerical simulations, additional data for the vortex ring creations, and stable vortex ring structures.
[41] J. H. C. Whitehead, Proc. Natl. Acad. Sci. U.S.A. **33**, 117 (1947).
[42] A. Vansteenkiste, J. Leliaert, M. Dvornik, M. Helsen, F. Garcia-Sanchez, and B. Van Waeyenberge, AIP Adv. **4**, 107133 (2014).
[43] G. P. Müller, M. Hoffmann, C. Dißelkamp, D. Schürhoff, S. Mavros, M. Sallermann, N. S. Kiselev, H. Jónsson, and S. Blügel, Phys. Rev. B **99**, 224414 (2019).
[44] Y. Fukumoto and Y. Hattori, J. Fluid Mech. **526**, 77 (2005).
[45] R. E. Hershberger, D. Bolster, and R. J. Donnelly, Phys. Rev. E **82**, 036309 (2010).
[46] S.-Z. Lin, J.-X. Zhu, and A. Saxena, Phys. Rev. B **99**, 140408(R) (2019).
[47] A. R. C. McCray, T. Cote, Y. Li, A. K. Petford-Long, and C. Phatak, Phys. Rev. Appl. **15**, 044025 (2021).
[48] J. C. Slonczewski, J. Magn. Magn. Mater. **159**, L1 (1996).
[49] L. Berger, Phys. Rev. B **54**, 9353 (1996).
[50] S. Zhang and Z. Li, Phys. Rev. Lett. **93**, 127204 (2004).
[51] M. Azhar, V. P. Kravchuk, and M. Garst, Phys. Rev. Lett. **128**, 157204 (2022).
[52] M. Sallermann, H. Jónsson, and S. Blügel, Phys. Rev. B **107**, 104404 (2023).
[53] D. Wolf, S. Schneider, U. K. Rößler, A. Kovács, M. Schmidt, R. E. Dunin-Borkowski, B. Büchner, B. Rellinghaus, and A. Lubk, Nat. Nanotechnol. **17**, 250 (2022).
[54] X. Yu, K. V. Iakoubovskii, F. S. Yasin, L. Peng, K. Nakajima, S. Schneider, K. Karube, T. Arima, Y. Taguchi, and Y. Tokura, Nano Lett. **22**, 9358 (2022).
[55] P. Fischer, D. Sanz-Hernández, R. Streubel, and A. Fernández-Pacheco, APL Mater. **8**, 010701 (2020).